Electronic Supplementary Material (ESI) for Journal of Materials Chemistry A.

Support Information

Realizing low ion migration and highly sensitive X-ray detection by building *g*-C_3N_4 and $CH_3NH_3PbI_3$ bulk heterojunction pellets

Chengzhi Xue,[a] Yingrui Xiao,[a] Xing Liu,[a] Ziwei Xu,[a] Nan Li,[a] Shubo Wang,[c] Ningyi Yuan,[d] Jianding Ding,[e] Xu Guo,*[a] Zhou Yang,*[a] and Shengzhong (Frank) Liu,*[ab]

a. Key Laboratory of Applied Surface and Colloid Chemistry, Ministry of Education; Shaanxi Key Laboratory for Advanced Energy Devices; Shaanxi Engineering Lab for Advanced Energy Technology; Institute for Advanced Energy Materials; School of Materials Science and Engineering, Shaanxi Normal University, Xi'an 710119, China. Email: szliu@dicp.ac.cn; zyang@snnu.edu.cn; guoxu@snnu.edu.cn
b. Dalian National Laboratory for Clean Energy; Dalian Institute of Chemical Physics, Chinese Academy of Sciences, Dalian116023, China
c. School of Chemical Engineering and Materials, Changzhou Institute of Technology, Changzhou, 213032 China
d. School of Materials Science and Engineering, Jiangsu Collaborative Innovation Center for Photovoltaic Science and Engineering, Jiangsu Province Cultivation Base for State Key Laboratory of Photovoltaic Science and Technology, Changzhou University, Changzhou, 213164 China
e. Micro/Nano Science and Technology Center, Jiangsu University, Zhenjiang, 212013 China

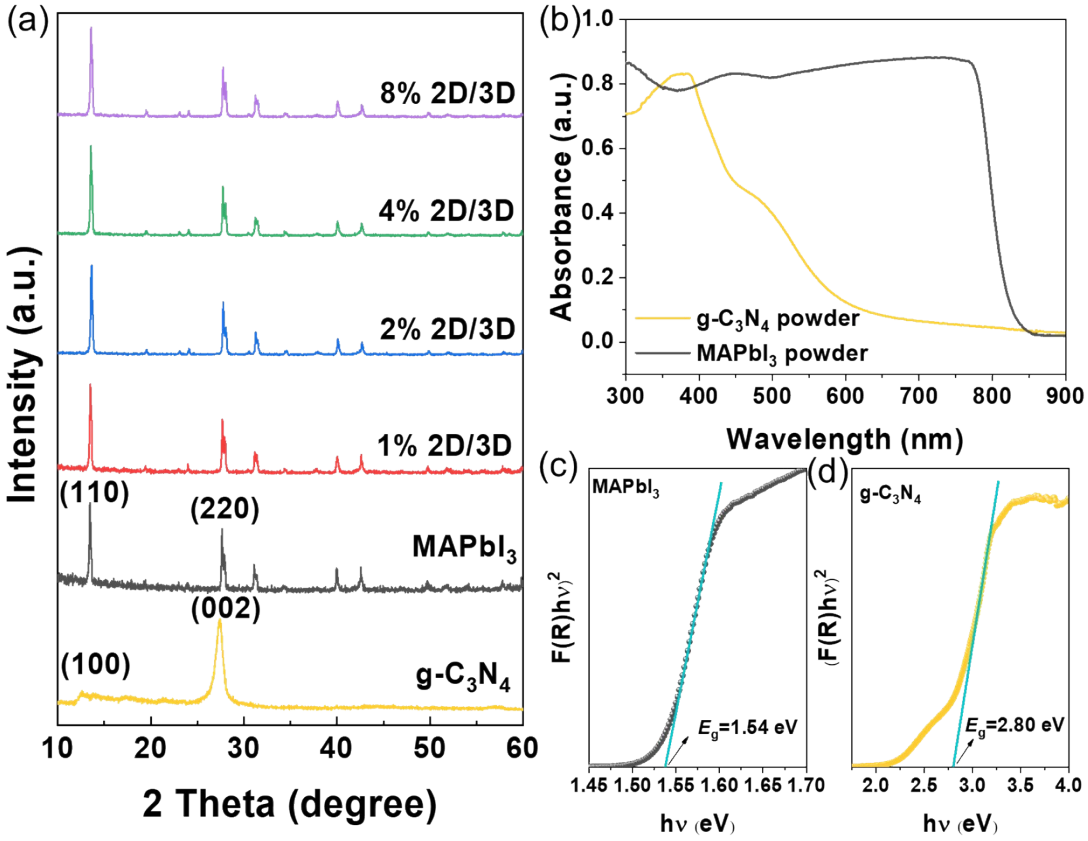

Fig. S1. (a) *g*-C_3N_4, $MAPbI_3$ powders and XRD diffractogram patterns of 2D/3D wafers. (b) UV-Vis absorption spectra of $MAPbI_3$ and *g*-C_3N_4. Band gap energy calculation (Tauc plots) (c) $MAPbI_3$, and (d) *g*-C_3N_4.

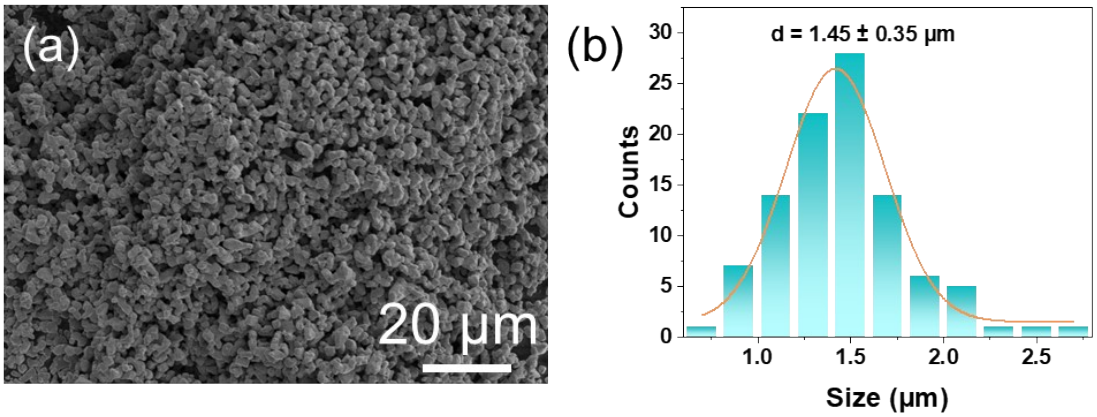

Fig. S2. (a) Scanning electron microscopy (SEM) images of the $MAPbI_3$ powder. (b) Grain size statistic of $MAPbI_3$ powders.

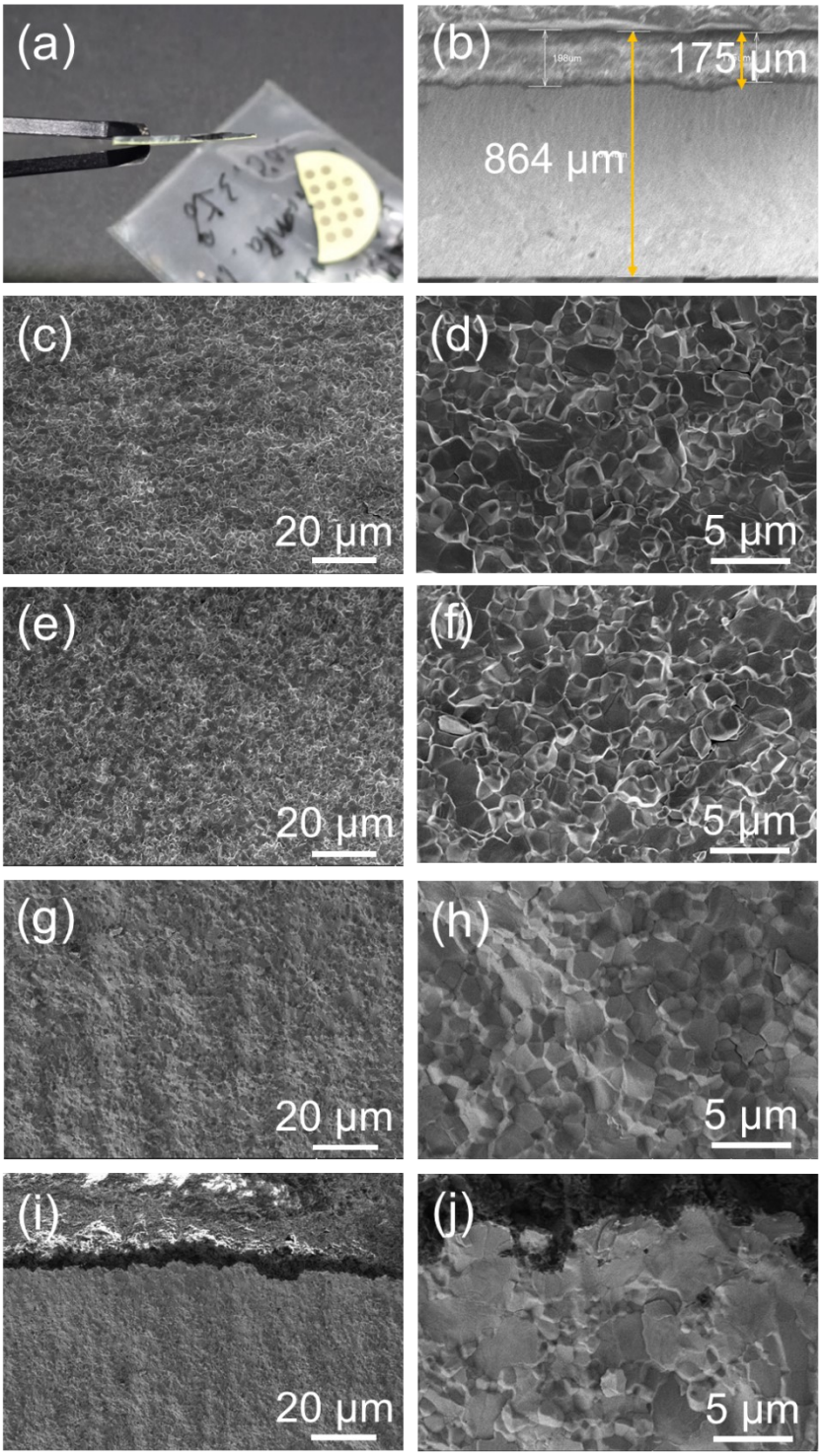

Fig. S3. Microstructure of perovskite and *g*-C_3N_4 double-layer wafer. (a, b) The cross-sectional thickness of the double-layer wafer and position of morphological enlargement. (c, d) Microstructure of the bottom of the perovskite layer. (e, f) Microstructure of the middle of the perovskite layer (g, h) Microstructure of the top of the perovskite layer. (i, j) Microstructure between the perovskite layer and the *g*-C_3N_4 layer.

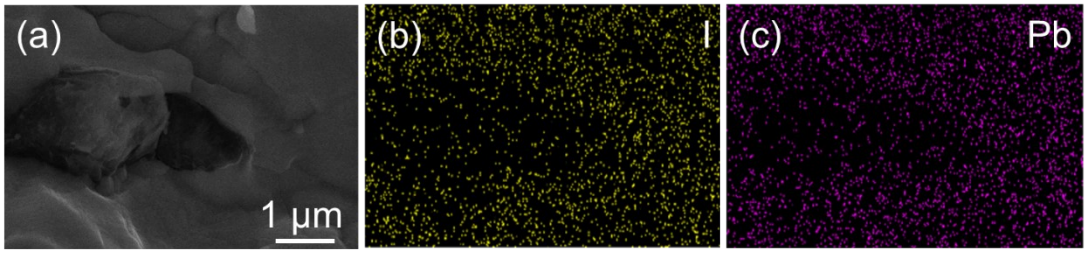

Fig. S4. Micro-regional elemental analysis of wafer cross-sections (a) Picture. Elemental distributions (b) I, and (c) Pb elements.

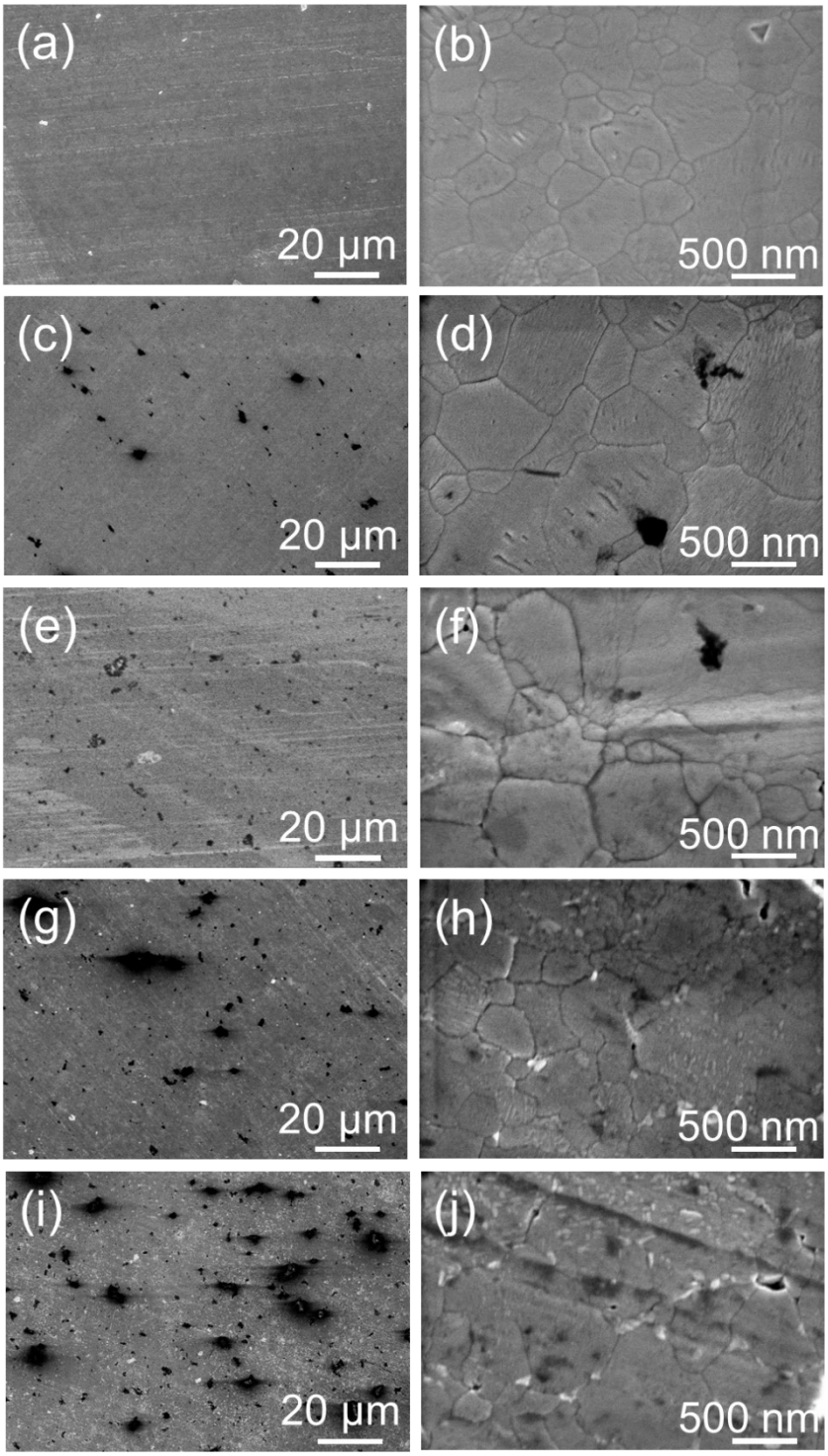

Fig. S5. The plane microstructure of the pellets. Scanning electron microscopy (SEM) images of the pristine 3D pellet (a, b), 1% 2D/3D pellet (c, d), 2% 2D/3D pellet (e, f), 4% 2D/3D pellet (g, h), and 8% 2D/3D pellet (i, j).

Fig. S6. Schematic diagram of wafer thickness.

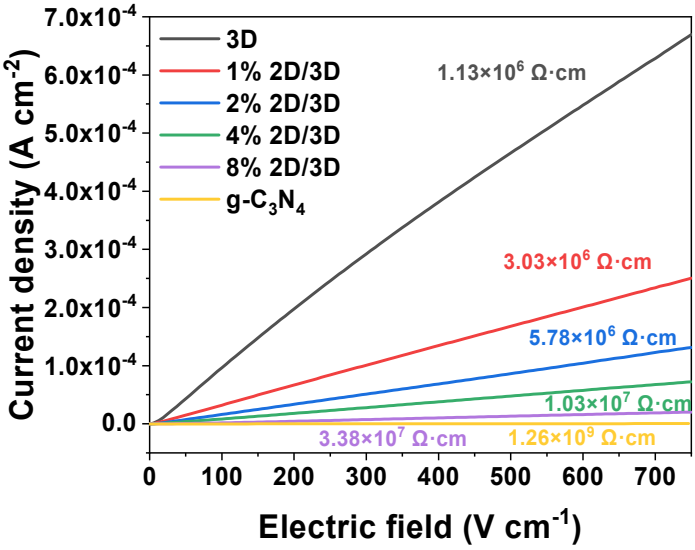

Fig. S7. Resistivities of 3D, 2D and 2D/3D wafers.

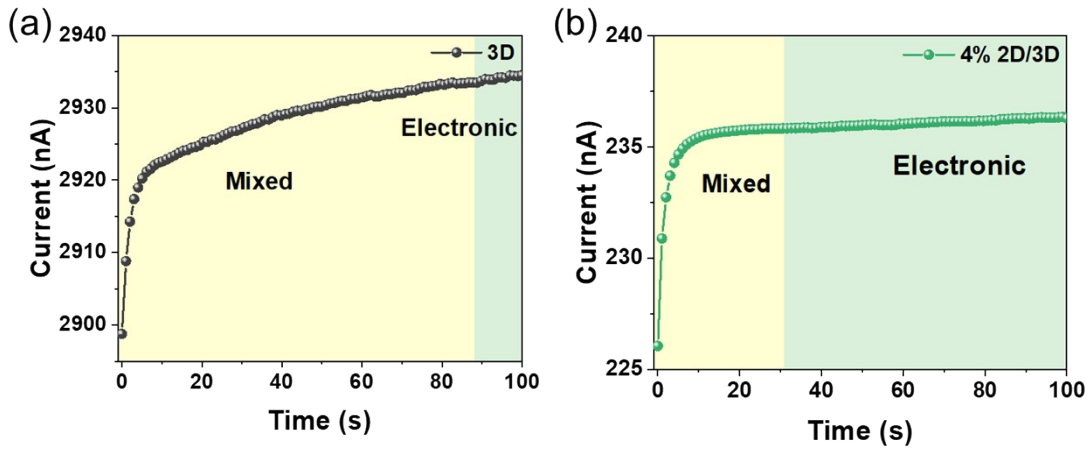

Fig. S8. Current time profile on the wafers at the beginning of the phase. Applying a voltage of 10 V. (a) 3D. (b) 4% 2D/3D. The mixed region in the diagram refers to the coexistence of both ionic and electronic conductivity. The electron region is where electron conductivity is dominant.

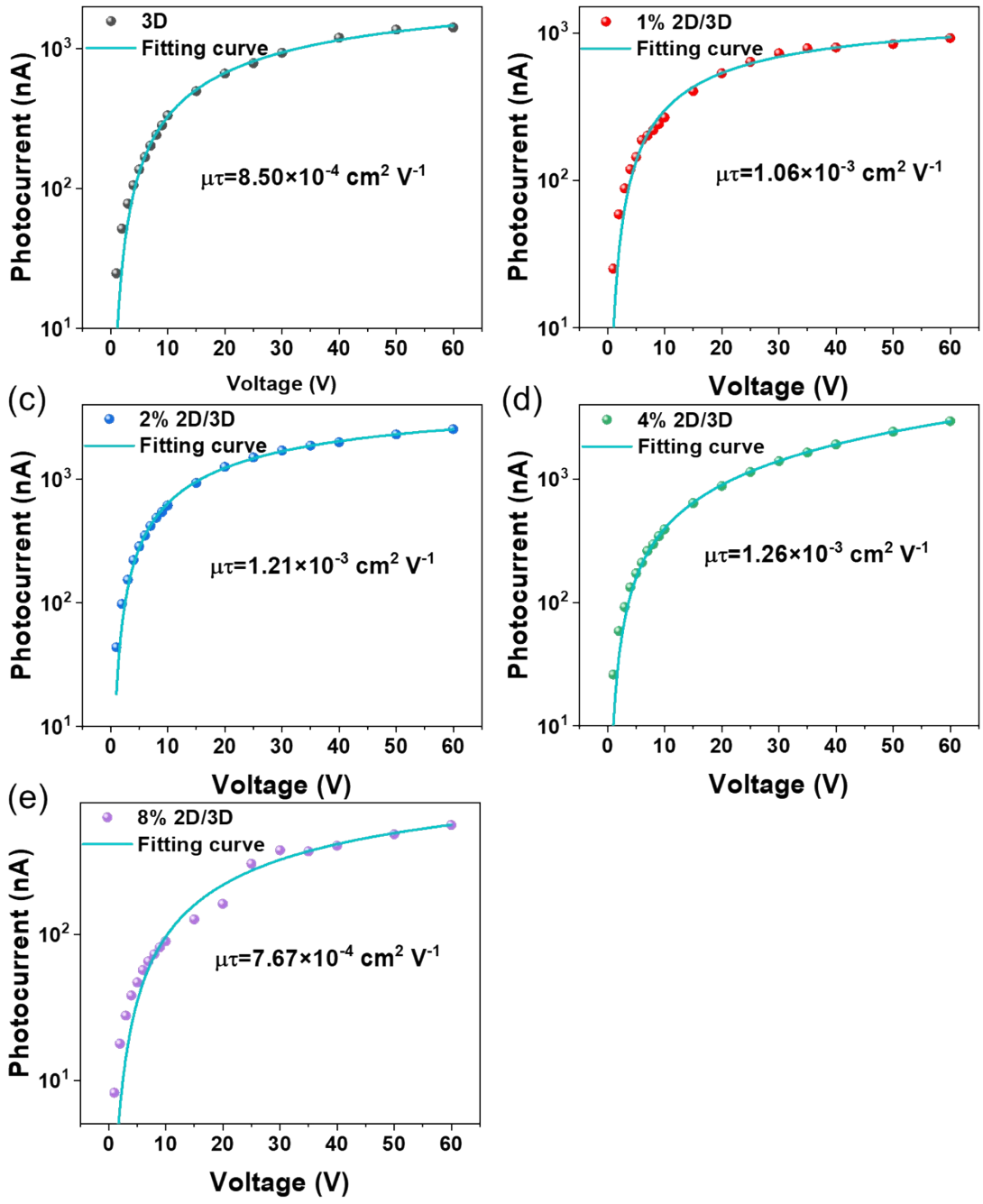

Fig. S9. Photoconductivity of 3D and 2D/3D wafers. Fitting lines for the $\mu\tau$ product were shown.

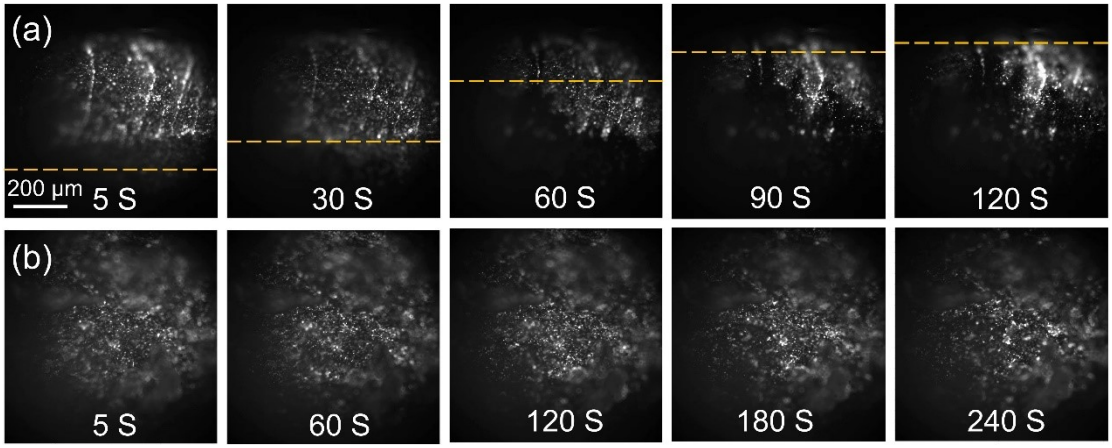

Fig. S10. The time-dependent PL mapping of (a) 3D wafer and (b) 4% 2D/3D wafer under 40 V bias and excitation of 405 nm laser.

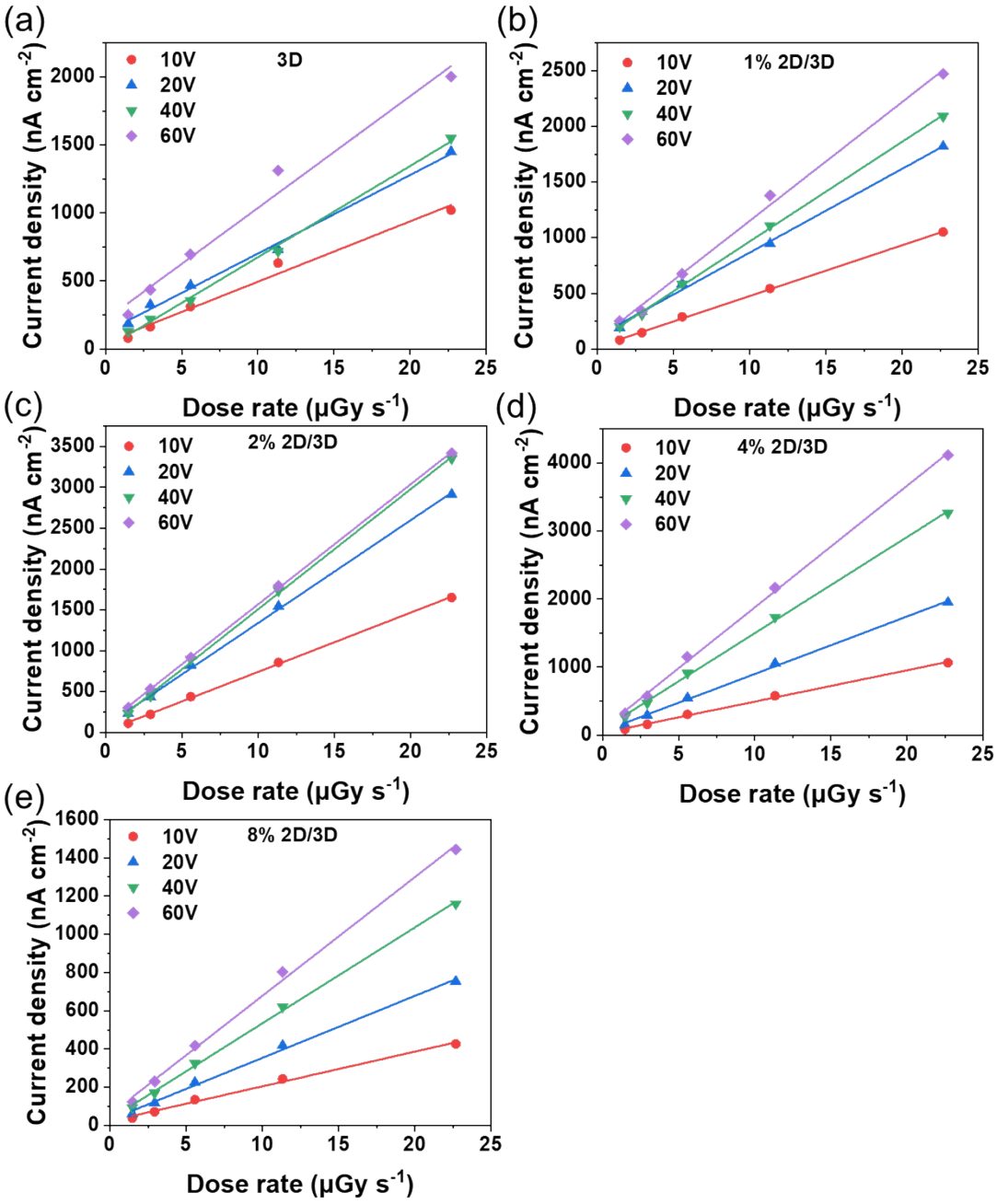

Fig. S11. Summary of response currents under different bias voltages and X-ray dose rates. (a) 3D, (b) 1% 2D/3D, (c) 2% 2D/3D, (d) 4% 2D/3D, and (e) 8% 2D/3D wafers.

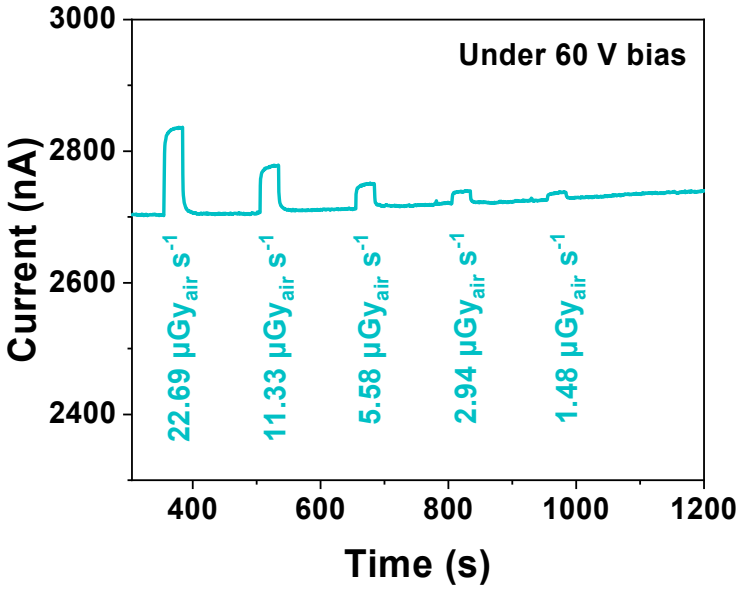

Fig. S12. 4% 2D/3D pellet response current and current drift at 60 V bias voltage.

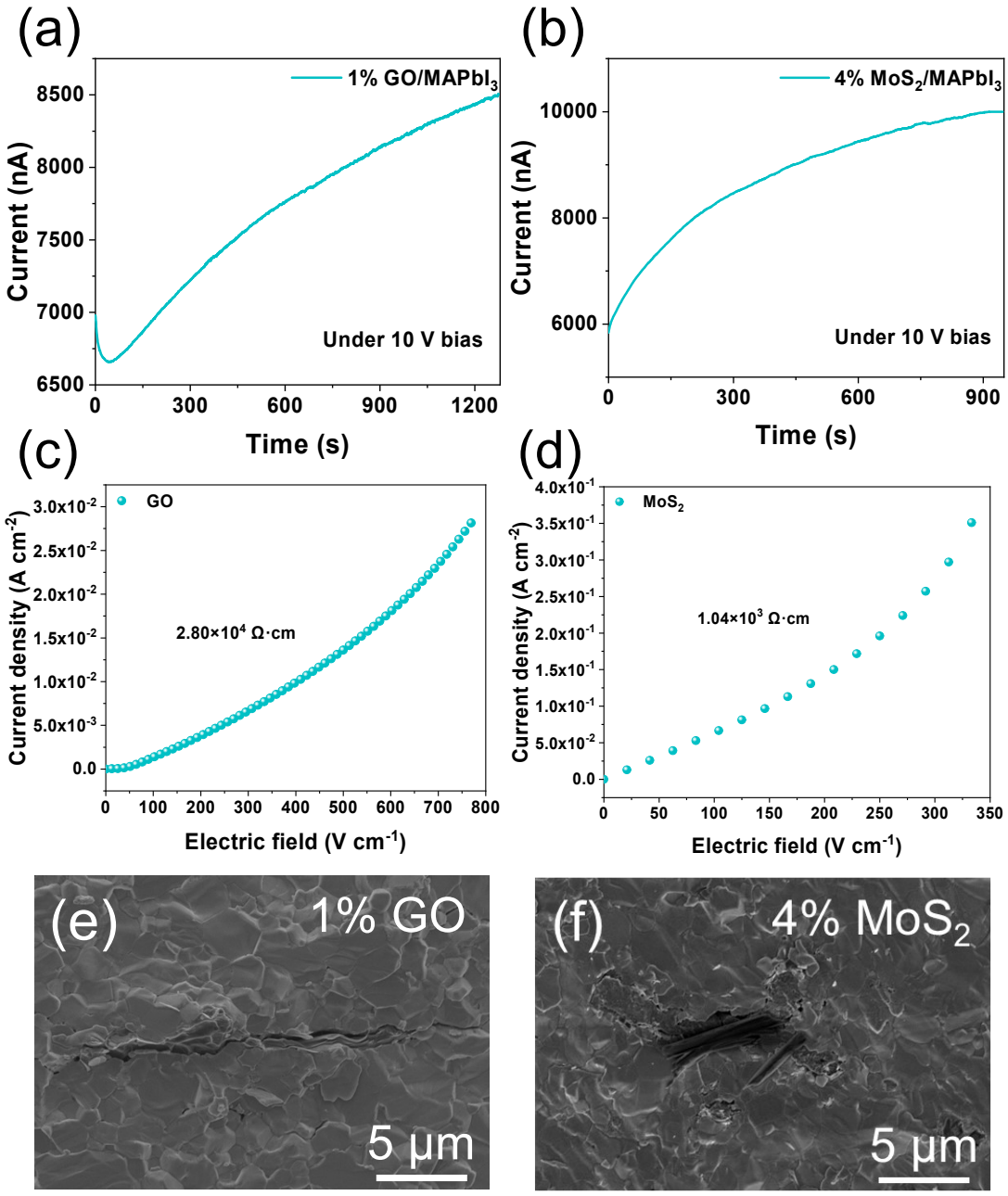

Fig. S13. Current-time curves for different 2D/3D mixed wafers at 10V bias. (a) 1% GO/$MAPbI_3$. (b) 4% MoS_2/$MAPbI_3$. Resistivities of the 1% GO/$MAPbI_3$ wafer (c), and 4% MoS_2/$MAPbI_3$ wafer (d). The cross-sectional microstructure of the pellets. Scanning electron microscopy (SEM) images of the 1% GO/$MAPbI_3$ pellet (c), and 4% MoS_2/$MAPbI_3$ pellet (d).

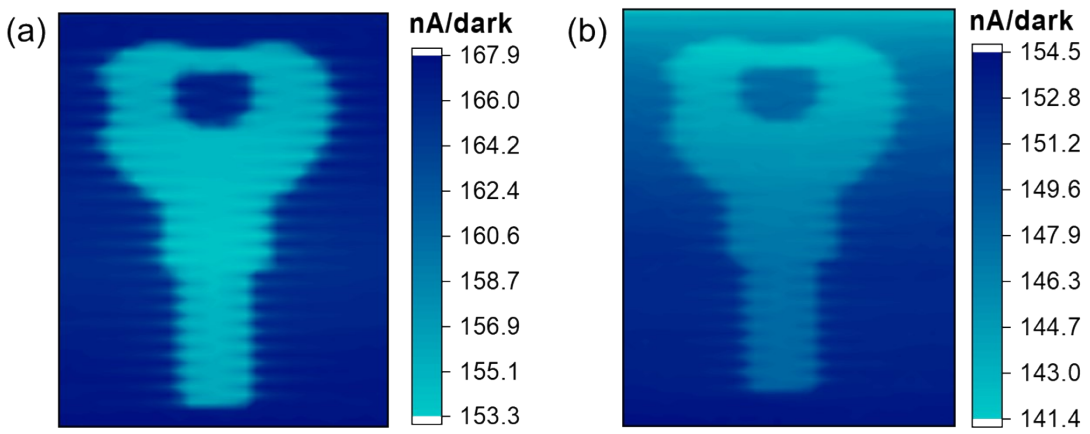

Fig. S14. X-ray image of the key obtained with a bias voltage of 10 V. (a) Dose rate of 11.57 μGy_{air} s^{-1}. (b) Dose rate of 5.698 μGy_{air} s^{-1}.

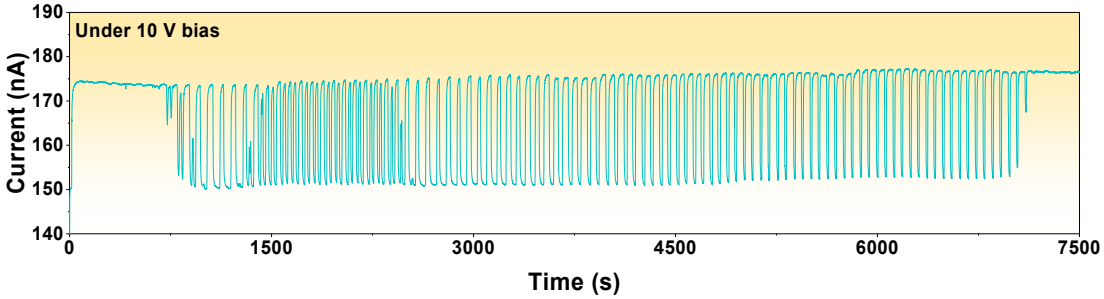

Fig. S15. The current-time curve of the imaging process.

Table S1. Summary of the dark current drift for reported perovskite-based X-ray or γ-ray detectors under different applied electric fields.

Materials	Applied electric field ($V\ cm^{-1}$)	Dark current drift ($nA\ cm^{-1}\ s^{-1}\ V^{-1}$)	References
3D $MAPbI_3$ single crystal	100	1.4×10^{-4}	[1]
3D $MAPbBr_3$ single crystal	20	1.2×10^{-3}	[2]
3D $CsPbBr_3$ single crystal	2000	1.9×10^{-4}	[3]
3D $MAPbI_3$ crystal with DPSI	270	1.2×10^{-5}	[4]
2D $(PEA)_2MA_3Pb_4I_{13}$-3D $MAPbI_3$ double-layer film	333	1.88×10^{-2}	[5]
3D $MAPbI_3$ film with PbI_2-DMSO powders	166.7	1.31×10^{-4}	[6]
2D BA_2PbI_4-3D $MAPbI_3$ bulk heterostructure pellet	125	4.84×10^{-5}	[7]
BiOBr passivated 3D $Cs_2AgBiBr_6$ film	5000	7.4×10^{-5}	[8]
2D $(F\text{-}PEA)_2PbI_4$ single crystal	1333	4.9×10^{-8}	[9]
2D $(BDA)PbI_4$ single crystal	4545	6.06×10^{-9}	[10]
4% 2D *g*-C_3N_4-3D $MAPbI_3$ bulk heterostructure pellet	126.6	4.02×10^{-4}	This work
8% 2D *g*-C_3N_4-3D $MAPbI_3$ bulk heterostructure pellet	126.6	4.87×10^{-5}	This work
3D $MAPbI_3$ polycrystalline pellet	126.6	1.13×10^{-2}	This work

Table S2. Summary of the sensitivity and *LoD* for reported perovskite-based X-ray detectors under different applied electric fields.

Materials	Applied electric field ($V\ cm^{-1}$)	Sensitivity ($\mu C\ Gy_{air}^{-1}\ cm^{-2}$)	Detection limit ($nGy_{air}\ s^{-1}$)	References
3D $MAPbI_3$ wafer	2000	2.5×10^3	N/A	[11]
3D $MAPbI_3$ film	2400	1.1×10^4	N/A	[12]
3D $MAPbI_3$ single crystal	1000	7.1×10^5	1.5	[13]
3D $MAPbI_3$ crystal with DPSI	417	2.9×10^6	5.7	[4]
3D $MAPbI_3$ microcrystalline	1700	9.3×10^3	N/A	[14]
2D $(PEA)_2MA_3Pb_4I_{13}$-3D $MAPbI_3$ double-layer film	333	1.9×10^4	480	[5]
3D $MAPbI_3$ film with PbI_2-DMSO powders	500	1.6×10^4	410	[6]
2D BA_2PbI_4-3D $MAPbI_3$ bulk heterostructure pellet	125	2.0×10^3	111.76	[7]
4% 2D *g*-C_3N_4-3D $MAPbI_3$ bulk heterostructure pellet	759.4	1.8×10^5	27	This work

References

1. S. Yakunin, D. N. Dirin, Y. Shynkarenko, V. Morad, I. Cherniukh, O. Nazarenko, D. Kreil, T. Nauser and M. V. Kovalenko, *Nat. Photonics*, 2016, **10**, 585-589.
2. W. Wei, Y. Zhang, Q. Xu, H. T. Wei, Y. J. Fang, Q. Wang, Y. H. Deng, T. Li, A. Gruverman, L. Cao and J. S. Huang, *Nat. Photonics*, 2017, **11**, 315.
3. Y. H. He, L. Matei, H. J. Jung, K. M. McCall, M. Chen, C. C. Stoumpos, Z. F. Liu, J. A. Peters, D. Y. Chung, B. W. Wessels, M. R. Wasielewski, V. P. Dravid, A. Burger and M. G. Kanatzidis, *Nat. Commun.*, 2018, **9**, 1609.
4. Y. Liu, X. P. Zheng, Y. J. Fang, Y. Zhou, Z. Y. Ni, X. Xiao, S. S. Chen and J. S. Huang, *Nat. Commun.*, 2021, **12**, 1686.
5. X. Xu, W. Qian, J. Wang, J. Yang, J. Chen, S. Xiao, Y. Ge and S. Yang, *Adv. Sci.*, 2021, **8**, 2102730.
6. W. J. Liu, T. Y. Shi, J. T. Zhu, Z. Y. Zhang, D. Li, X. C. He, X. S. Fan, L. Q. Meng, J. H. Wang, R. He, Y. S. Ge, Y. L. Liu, P. K. Chu and X. F. Yu, *Adv. Sci.*, 2023, **10**, 2204512.
7. Y. Xiao, C. Xue, X. Wang, Y. Liu, Z. Yang and S. Liu, ACS Appl. Mater. Interfaces, 2022, 14, 54867-54875.
8. B. Yang, W. C. Pan, H. D. Wu, G. D. Niu, J. H. Yuan, K. H. Xue, L. X. Yin, X. Y. Du, X. S. Miao, X. Q. Yang, Q. G. Xie and J. Tang, *Nat. Commun.*, 2019, **10**, 1989.
9. H. Y. Li, J. M. Song, W. T. Pan, D. R. Xu, W. A. Zhu, H. T. Wei and B. Yang, Adv. Mater., 2020, 32, 2003790.
10. Y. Shen, Y. Liu, H. Ye, Y. Zheng, Q. Wei, Y. Xia, Y. Chen, K. Zhao, W. Huang and S. Liu, *Angew. Chem. Int. Ed.*, 2020, **59**, 14896-14902.
11. S. Shrestha, R. Fischer, G. J. Matt, P. Feldner, T. Michel, A. Osvet, I. Levchuk, B. Merle, S. Golkar, H. W. Chen, S. F. Tedde, O. Schmidt, R. Hock, M. Ruhrig, M. Goken, W. Heiss, G. Anton and C. J. Brabec, *Nat. Photonics*, 2017, **11**, 436.
12. Y. C. Kim, K. H. Kim, D. Y. Son, D. N. Jeong, J. Y. Seo, Y. S. Choi, I. T. Han, S. Y. Lee and N. G. Park, *Nature*, 2017, **550**, 87.
13. Y. L. Song, L. Q. Li, W. H. Bi, M. W. Hao, Y. F. Kang, A. R. Wang, Z. S. Wang, H. M. Li, X. H. Li, Y. J. Fang, D. R. Yang and Q. F. Dong, *Research*, 2020, **2020**, 5958243.
14. S. Deumel, A. van Breemen, G. Gelinck, B. Peeters, J. Maas, R. Verbeek, S. Shanmugam, H. Akkerman, E. Meulenkamp, J. E. Huerdler, M. Acharya, M. Garcia-Batlle, O. Almora, A. Guerrero, G. Garcia-Belmonte, W. Heiss, O. Schmidt and S. F. Tedde, *Nat. Electron.*, 2021, **4**, 681-688.